IEEE Access
Multidisciplinary ⋮ Rapid Review ⋮ Open Access Journal

Received April 26, 2020, accepted May 19, 2020, date of publication May 25, 2020, date of current version June 5, 2020.

Digital Object Identifier 10.1109/ACCESS.2020.2996948

Integration of FOC With DFVC for Interior Permanent Magnet Synchronous Machine Drives

TIANFU SUN[1,2,3], (Member, IEEE), JIABIN WANG[4], (Senior Member, IEEE), CHENGLI JIA[1], AND LEI PENG[1,2], (Member, IEEE)

[1]Shenzhen Institutes of Advanced Technology, Chinese Academy of Sciences, Shenzhen 518055, China
[2]Shenzhen Key Laboratory of Electric Vehicle Powertrain Platform and Safety Technology, Shenzhen 518055, China
[3]CAS Key Laboratory of Human–Machine Intelligence-Synergy Systems 518055, China
[4]Department of Electronics and Electrical Engineering, The University of Sheffield, Sheffield S10 2TN, U.K.

Corresponding author: Tianfu Sun (tianfu.sun@foxmail.com)

This work was supported in part by the Chinese National Natural Science Foundation of China (NSFC) under Grant 51707191, in part by the Technique Development Plan of Guangdong Province under Grant 2019B090917001, in part by the Shenzhen Basic Research Program under Grant JCYJ20180507182619669, Grant JCYJ20170818164527303, and Grant JCYJ20180507182628567, and in part by the Shenzhen Institutes of Advanced Technology (SIAT) Outstanding Youth Fund under Grant Y8G020.

ABSTRACT In this paper, the drawbacks of the conventional f-t frame based maximum torque per ampere (MTPA) control schemes are analyzed and mathematically proved. In order to inherit the merits of both the direct flux vector control (DFVC) in field weakening region and field orientated control (FOC) in constant torque region while avoiding their disadvantages, an integrated control scheme is proposed. The proposed control scheme integrates the FOC into f-t reference frame at low speeds to achieve a relatively accurate and robust MTPA control, while at high speeds, the DFVC is adopted to utilize the advantages of f-t frame based control scheme in field weakening region. A shape function is utilized by the proposed control scheme to achieve a smooth transition between the two control schemes. The proposed control scheme is verified by experiments under various operation conditions on a prototype IPMSM drive. The simulation and experimental results illustrate that the proposed control scheme could achieve a better MTPA control accuracy in constant torque region and a better field weakening performance in the constant power region. Meanwhile the complex look-up tables for FOC in field weakening region and the difficulties in observing flux vector at low speed are avoided.

INDEX TERMS Maximum torque per ampere (MTPA) control, direct flux vector control (DFVC), field orientated control (FOC), interior permanent magnet synchronous machine (IPMSM), torque control.

I. INTRODUCTION

Interior permanent magnet synchronous machines (IPMSM) have many attractive advantages such as high efficiency, high power/torque density [1]–[3], high reliability and good field-weakening performance [1], [4], therefore, it has been used in plenty of industrial applications, such as robot motion control, electric vehicles and other industrial fields [5], [6]. In order to control IPMSM drives, in literature, both field orientated control (FOC) in the rotor reference (d-q) frame [7]–[9] and direct flux vector control (DFVC) in the flux-torque (f-t) reference frame [10]–[13] have been proposed to achieve MTPA control in constant torque region [14], [15] and field weakening operation in constant power region [16], [17]. In the FOC, the d- and q-axis currents are regulated by the d- and q-axis PI controllers [18], [19]. Since the d- and q-axis currents can be obtained from measured phase currents and rotor position, the FOC can track the optimal d- and q-axis current commands accurately in constant torque region. Therefore, the accurate MTPA operation can be easily achieved [2]. In the field weakening region, however, due to the voltage limit, the stator flux amplitude should be limited, and this limit is indirectly imposed by setting d-axis current demand as functions of torque and speed based on a machine model. Since the machine parameters of an IPMSM are highly nonlinear and vary with cross-coupling effects, magnetic saturation and temperature [20], [21], it is difficult to achieve optimal field weakening control that satisfies the voltage constraint while maximizing efficiency. Moreover, dc-link voltage variations, which could be quite

The associate editor coordinating the review of this manuscript and approving it for publication was Zhong Wu.

significant in electric vehicle traction drives supplied from batteries, also cause great difficulties in controlling IPMSM in field weakening region. Consequently, the performance of the FOC is compromised in field weakening operation.

On the other hand, the f-t frame based DFVC schemes directly regulates the stator flux amplitude by the f-axis voltage and controls the torque by the t-axis voltage through PI controllers [13], [22], [23]. At high speeds, the flux amplitude can be estimated by a voltage model based flux observer with relatively high accuracy [24]. Moreover, in the field weakening region, the maximum reference flux amplitude under voltage constraint can be calculated without machine parameters except for stator resistance [25]. Since the voltage drop across the phase resistance is very small compared with the maximum voltage, the stator resistance can be assumed to its nominal value without compromising the observer accuracy. Therefore, the f-t frame based control schemes are not only robust to dc-link voltage variations in field weakening region but also can directly impose the stator flux amplitude limit, thus they have a better performance than the FOC in field weakening region [12]. However, the performance of f-t frame based control schemes is highly dependent on the quality of a flux observer. At low speeds, especially when the speed is close to zero, due to the inverter parameter uncertainty, error of winding resistance estimation and relatively small voltage amplitude, the voltage model based observer is no longer accurate and a current model based observer is often employed [26]. Since current model based observers rely on the machine model for stator flux estimation, the nonlinearity of the machine parameters and inaccuracy of the machine model greatly affects the quality of current model based flux observers. Moreover, due to the difficulties of measuring the flux amplitude, the optimal flux amplitude for MTPA operation cannot be obtained accurately. Therefore, in constant torque region when speed is relatively low, the f-t frame based MTPA control schemes are more vulnerable to command and flux observer errors compared with the FOC scheme, and the FOC scheme is more desirable than the control schemes in the f-t frame when the motor operates at low speed.

In order to utilize the advantages of the FOC at low speeds and the advantages of f-t frame based control schemes at high speeds, while avoid their drawbacks, an integrated control scheme which combines the two kinds control schemes is proposed in this paper. At low speeds, the FOC is adopted, whereas at high speeds, the direct flux vector control (DFVC) scheme [13], [22], [23], [27] is employed as a kind of f-t frame based control scheme. In this way, the proposed control scheme could achieve a better efficiency optimization control accuracy in constant torque region and a better field weakening performance in constant power region. Meanwhile the complex look-up tables for FOC in field weakening region and the difficulties in observing flux vector at low speed can be avoided.

The rest of this paper is organized as follows: Section II mathematically proves the sensitivity of the existing f-t frame based control schemes to the errors in flux amplitude for MTPA control and the unique mapping between (Ψ_s, i_t) and $(i_d i_q)$. Section III details the method to implement the proposed integrated control scheme. Section IV and V provide the simulation and experimental verifications of the proposed control scheme in a variety of operation conditions, respectively. The conclusions are drawn in Section VI.

II. PRINCIPLE OF THE PROPOSED INTEGRATED CONTROL SCHEME

A. SENSITIVITY OF F-T FRAME BASED CONTROL SCHEMES TO ERRORS IN REFERENCE FLUX AMPLITUDE FOR MTPA CONTROL

The relationships between d- and q-axis currents, i_d, i_q, and d- and q-axis flux amplitudes, Ψ_d, Ψ_q, are given in (1) and (2), where L_d, L_q and Ψ_m are the d- and q-axis inductances and the flux linkage due to permanent magnets, respectively.

$$\Psi_d = L_d i_d + \Psi_m \tag{1}$$
$$\Psi_q = L_q i_q \tag{2}$$

According to (1) and (2), the flux amplitude, Ψ_s, for MTPA operation can be expressed in (3).

$$\begin{aligned}\Psi_s &= \sqrt{(\Psi_d)^2 + \left(\Psi_q\right)^2} \\ &= \sqrt{(\Psi_m + L_d i_d)^2 + \left(L_q i_q\right)^2}\end{aligned} \tag{3}$$

If the d-axis current in (3) contains a small error, Δi_d, the corresponding flux amplitude error, $\Delta\Psi_s$, can be expressed in (4).

$$\Psi_s + \Delta\Psi_s = \sqrt{\left[\Psi_m + L_d\left(i_d + \Delta i_d\right)\right]^2 + \left(L_q i_q\right)^2} \tag{4}$$

(3) minus (4) leads to (5):

$$\begin{aligned}&2\left(\Psi_s + 0.5\Delta\Psi_s\right)\Delta\Psi_s \\ &\qquad = 2\left[\Psi_m + L_d\left(i_d + 0.5\Delta i_d\right)\right] L_d \Delta i_d\end{aligned} \tag{5}$$

Since Δi_d is small compared with i_d and $\Delta\Psi_s$ is small compared with Ψ_s, (5) can be approximated by (6).

$$\Psi_s \Delta\Psi_s \approx \left[\Psi_m + L_d i_d\right] L_d \Delta i_d = \Psi_d L_d \Delta i_d \tag{6}$$

(6) is equivalent to (7).

$$\frac{\Delta\Psi_s}{\Psi_s} \approx \frac{\Psi_d}{\Psi_s}\frac{\left(L_d i_d\right)}{\Psi_s}\frac{\Delta i_d}{i_d} \tag{7}$$

Since $\Psi_s > \Psi_d$ and $\Psi_s \gg (L_d i_d)$, $\Delta i_d / i_d$ will be much larger than $\Delta\Psi_s/\Psi_s$, which means a relatively small error in the flux amplitude would lead to a relatively large error in the d-axis current and vice versa. This will be experimentally proved in Section V (Fig. 14 and Fig. 15).

Therefore, the MTPA operation is robust to errors in the d-axis current but very sensitive to errors in the flux amplitude. Since the reference and the observed flux always contain errors, the accurate MTPA operations are always more difficult to be guaranteed in the f-t frame. Therefore, for MTPA operation, the FOC is preferred.

B. MATHEMATICAL MODEL OF IPMSM

In field oriented control scheme, the MTPA control can be realized by setting the reference d- and q-axis currents to the optimal values and the d- and q-axis currents can be accurately controlled to follow the optimal reference currents through two current feedback loops. The mathematical model of the field oriented control method is expressed in (8) to (10). Where v_d and v_q are the d- and q-axis voltages, R is the stator resistance, p is the number of pole pairs, T_e is the electromagnetic torque and ω_m is rotor angular speed.

$$v_q = L_q \frac{di_q}{dt} + Ri_q + p\omega_m L_d i_d + p\omega_m \Psi_m \tag{8}$$

$$v_d = L_d \frac{di_d}{dt} + Ri_d - p\omega_m L_q i_q \tag{9}$$

$$T_e = \frac{3p}{2}[\Psi_m i_q + (L_d - L_q)\, i_q i_d] \tag{10}$$

Alternatively, the mathematical model of an IPMSM can also be expressed in (11) to (15) together with the current and flux amplitude limits in the f-t reference frame. Where v_f and v_t are the f- and t-axis voltages, i_f and i_t are the f- and t-axis currents, respectively. Ψ_s is the stator flux vector amplitude, and the torque angle, δ, is the angle of the stator flux vector with respect to the d-axis. I_{lim} is the current limit.

$$v_f = Ri_f + \frac{d\Psi_s}{dt} \tag{11}$$

$$v_t = Ri_t + \Psi_s \left(p\omega_m + \frac{d\delta}{dt}\right) \tag{12}$$

$$T_e = \frac{3}{2} p \Psi_s i_t \tag{13}$$

$$\sqrt{I_{lim}^2 - i_f^2} \geq i_t \tag{14}$$

$$\frac{1}{p\omega_m}\left[\sqrt{v_{lim}^2 - \left(Ri_f\right)^2} - Ri_t\right] \geq \Psi_s \tag{15}$$

The relationships between the d-q frame quantities and the f-t frame quantities are given in (16) to (18).

$$\delta = actan(\frac{\Psi_q}{\Psi_d}) \tag{16}$$

$$i_t = i_q \cos\delta - i_d \sin\delta \tag{17}$$

$$i_f = i_d \cos\delta + i_q \sin\delta \tag{18}$$

C. THE UNIQUE MAPPING BETWEEN (Ψ_s, i_t) AND (i_d, i_q)

Before the combination of the two control schemes formulated in the d-q and f-t reference frames, a discussion of the relationship between the d-q frame based control and the f-t frame based control is necessary. In steady state if the voltage drop on the phase resistance is neglected, the d- and q-axis voltages, v_d, v_q, can be simplified as (19) and (20).

$$v_q = p\omega_m L_d i_d + p\omega_m \Psi_m \tag{19}$$

$$v_d = -p\omega_m L_q i_q \tag{20}$$

Based on (19) and (20), the relationship between voltage amplitude, v_a, and d- and q-axis currents can be approximated by (21) and the relationship between v_a and flux amplitude, Ψ_s, can be approximated by (22).

$$v_a^2 = \left(p\omega_m L_q i_q\right)^2 + \left(p\omega_m L_d i_d + p\omega_m \Psi_m\right)^2 \tag{21}$$

$$v_a = p\omega_m \Psi_s \tag{22}$$

By substitution of (22) into (21):

$$\frac{\left(i_d + \frac{\Psi_m}{L_d}\right)^2}{\left(\frac{\Psi_s}{L_d}\right)^2} + \frac{i_q^2}{\left(\frac{\Psi_s}{L_q}\right)^2} = 1 \tag{23}$$

(21) is an ellipse. This ellipse is the constant flux amplitude locus.

Substitution of (10) and (13) into (23) leads to (24) which is a quartic equation about i_d. Therefore, for a given Ψ_s and i_t, i_d can be obtained by solving (24) and the i_q can be obtained through (10) based on the roots of (24).

$$\frac{\left(i_d + \frac{\Psi_m}{L_d}\right)^2}{\left(\frac{\Psi_s}{L_d}\right)^2} + \frac{\left(\frac{\Psi_s i_t}{[\Psi_m + (L_d - L_q) i_d]}\right)^2}{\left(\frac{\Psi_s}{L_q}\right)^2} = 1 \tag{24}$$

For easier expression, the diagram of constant flux amplitude loci and constant torque loci (given in (10)) in d-q frame are shown in Fig. 1. It worth to be noticed that according to (10), a constant torque locus actually contains two parts, one is across the first and second quadrants of Fig. 1, the other is in the fourth quadrant. However, since motors are always operated in the second quadrant, the constant torque locus in the fourth quadrant is always ignored.

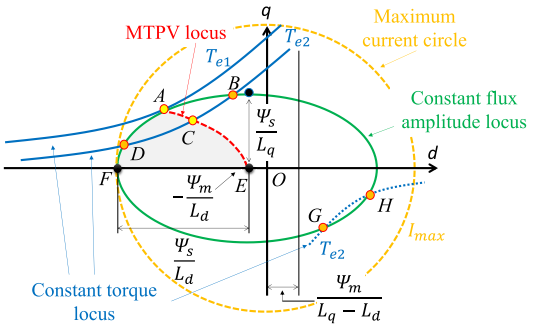

FIGURE 1. Constant flux amplitude locus, current limit circle, MTPV locus and constant torque locus with the possible roots of (24).

The center of the constant flux amplitude loci is at the point $(-\Psi_m/L_d, 0)$. The tangential point between a constant torque locus and a constant flux amplitude locus, e.g., point A, is the maximum torque per voltage (MTPV) point [13]. The MTPV locus, *A-C-E*, is also shown in Fig. 1.

As shown in Fig. 1, the quartic equation given in (24) at most has four roots which are the intersections between the constant torque locus and the constant flux amplitude locus, e.g., the points *B*, *D*, *G*, and *H* in Fig. 1. However, the point on the left hand side of the MTPV locus, i.e., point *D*, and the points in the fourth quadrant, i.e., points *G* and *H*, should be avoided by limiting the δ as mentioned in [13]. Since the

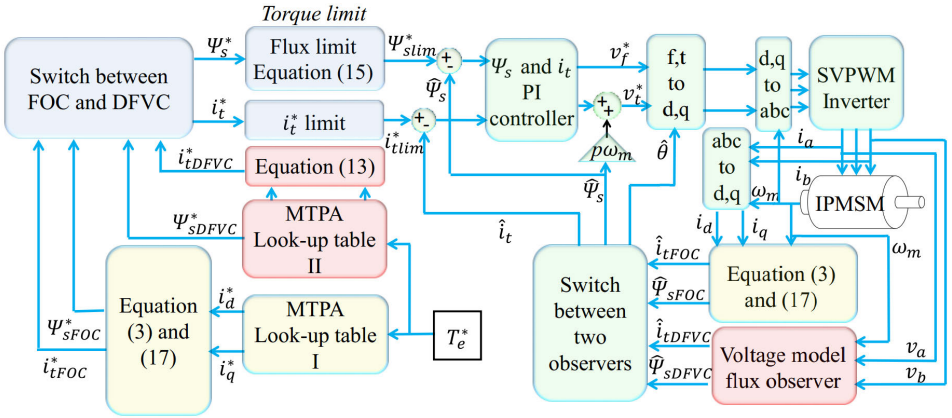

FIGURE 2. Block diagram of the proposed control scheme.

motor should be controlled either on the right hand side of the MTPV locus or right on the MTPV locus in the first quadrant, the relationship between Ψ_s, i_t and i_d, i_q under the direct flux vector control is unique.

In direct flux vector control, as mentioned in [13], [22], [23], the motor's flux amplitude and t-axis current are controlled through the f- and t-axis voltages. The observed flux amplitude, $\hat{\Psi}_s$, and t-axis current, $\hat{i}_t$, can be expressed in (25) and (26) with measured i_d and i_q, respectively.

$$\hat{\Psi}_s^2 = (L_d i_d + \Psi_m)^2 + (L_q i_q)^2 \tag{25}$$

$$\hat{i}_t = \frac{\frac{3p}{2}[\Psi_m i_q + (L_d - L_q) i_q i_d]}{\hat{\Psi}_s} \tag{26}$$

In steady state, the observed flux amplitude and t-axis current should equal the reference flux amplitude Ψ_s^* and the reference t-axis current i_t^*, respectively, as expressed in (27) and (28).

$$\hat{\Psi}_s^2 = \Psi_s^{*2} = (L_d i_d^* + \Psi_m)^2 + (L_q i_q^*)^2 \tag{27}$$

$$\hat{i}_t = i_t^* = \frac{\frac{3p}{2}[\Psi_m i_q^* + (L_d - L_q) i_q^* i_d^*]}{\Psi_s^*} \tag{28}$$

Due to the unique relationship between Ψ_s, i_t and i_d, i_q under direct flux vector control, for one pair of Ψ_s^* and i_t^*, in steady state, there is only one pair of achievable d- and q-axicurrents. Therefore, according to (25) to (28), $i_d = i_d^*$ and $i_q = i_q^*$. In other words, the d- and q-axis currents can be controlled to follow i_d^* and i_q^* through Ψ_s^* and i_t^*. It should be noticed that if the machine parameters in (25) to (28) are their nominal values, the resultant Ψ_s^*, $\hat{\Psi}_s$ and i_t^*, $\hat{i}_t$ will also be their nominal values. However, the unique relationship between a pair of flux amplitude and t-axis current and the pair of d- and q-axis currents in Fig. 1 still exists, and errors in observed or reference flux amplitude and t-axis current will not affect the accuracy of the d- and q-axis current control under the condition that the machine parameters in (25) to (28) are the same. This will be proved by simulations in Section IV (Fig. 6).

III. IMPLEMENTATION OF THE PROPOSED CONTROL SCHEME

Since the FOC is more robust than f-t frame based control schemes for MTPA operation meanwhile the f-t frame based control schemes have advantages over the FOC in field weakening region, in order to take the advantages of FOC for MTPA operation and the advantages of f-t frame based control schemes for filed weakening operation while avoiding their weaknesses, an integrated control scheme is proposed in which FOC is employed at low speed (MTPA control) and the direct flux vector control [13], [22], [23], a kind of f-t frame based control scheme, is adopted at high speed (field weakening control). The schematic of the proposed control scheme is shown in Fig. 2. Seamless transitions between the two control strategies are realized by adopting a unified control structure in the form of the DFVC.

As shown in Fig. 2, the proposed control scheme consists of two main control loops, the stator flux control loop and the t-axis current control loop. Limits on the Ψ_s^* and i_t^* are imposed in the same manner as described in [13], [22], [23]. However, Ψ_s^* and i_t^* can either be generated from reference d- and q-axis currents via the MTPA Look-up table 1 for FOC or from MTPA Look-up table 2 and (13) for DFVC, depending on rotor speeds. The details of the proposed control scheme will be discussed below.

A. FOC FOR MTPA OPERATION

As shown in Fig. 2, for a given torque command, T_e^*, the MTPA Look-up table generates the corresponding optimal reference d- and q-axis current commands, i_d^* and i_q^*, for MTPA operation. The resultant optimal i_d^* and i_q^* will be further converted into Ψ_{sFOC}^* and i_{tFOC}^* through (1) to (3) and (17) based on the nominal machine parameters, L_d, L_q, Ψ_m of the machine. If the motor speed ω_m is below a pre-defined value ω_1, the reference flux amplitude and t-axis

current (Ψ_s^*, i_t^*) will equal (Ψ_{sFOC}^*, i_{tFOC}^*) and the observed flux amplitude and t-axis current ($\hat{\Psi}_s$, $\hat{i}_t$) will equal ($\hat{\Psi}_{sFOC}$, $\hat{i}_{tFOC}$) which is calculated by (1) to (3) and (17) based on the measured d- and q-axis current (i_d,i_q) with the same machine parameters of the calculation of (Ψ_{sFOC}^*, i_{tFOC}^*). In this way, the Ψ_s and i_t controllers in Fig. 2 will control the ($\hat{\Psi}_{sFOC}$, $\hat{i}_{tFOC}$) to follow the (Ψ_{sFOC}^*, i_{tFOC}^*). Due to the unique mapping between (Ψ_{sFOC}^*, i_{tFOC}^*) and (i_d^*, i_q^*) as well as the unique relationship between ($\hat{\Psi}_{sFOC}$, $\hat{i}_{tFOC}$) and (i_d, i_q), when ($\hat{\Psi}_{sFOC}$, $\hat{i}_{tFOC}$) equals (Ψ_{sFOC}^*, i_{tFOC}^*) in steady state, the measured d- and q-axis currents (i_d, i_q) will be equal to the reference d- and q-axis currents, (i_d^*, i_q^*). Therefore, the d- and q-axis currents can be controlled through the f-t frame. This control scheme essentially controls the d- and q-axis currents and equivalent to the FOC. In this way, the sensitivity of the MTPA control to the reference flux amplitude and flux observer errors in f-t frame can be avoided and the optimal d- and q-axis currents can be easily and accurately obtained through experiments or other online MTPA control schemes [28]. Moreover, as mentioned in Section II Part C, small errors of the nominal machine parameters in (3) and (17) will not affect the controlling of the d- and q-axis currents.

However, in field weakening region, the stator flux amplitude is difficult to be limited accurately due to the flux estimation errors of (3) and (17) and the reference d- and q-axis currents generated from Look-up table 1 are difficult to cope with the dc-link voltage variations. This will deteriorate field weakening performance. Therefore, at high speed, especially for field weakening control, DFVC is preferable.

B. DFVC FOR FIELD WEAKENING CONTROL

In order to overcome the problems associate the FOC, the DFVC is adopted at relatively high speeds, however, other kinds of f-t frame based control schemes are also possible.

When the motor operates at high speeds, the voltage drops on the stator resistance and inverter are relatively small compared with the voltage amplitude, the stator resistance and the inverter parameters can be assumed as its nominal value and the accuracy of the voltage model flux observer can be guaranteed. In this case, as shown in Fig. 2, when ω_m is above a pre-defined value ω_2 which is close to the base speed, the proposed control scheme switches to the conventional DFVC proposed in [13], [22], [23],. The optimal reference flux amplitude, Ψ_{sDFVC}^*, and the reference t-axis current, i_{tDFVC}^*, for MTPA control are generated from the Look-up table 2 and (13) with the reference torque as its input. (Ψ_s^*, i_t^*) is equal to (Ψ_{sDFVC}^*, i_{tDFVC}^*) while ($\hat{\Psi}_m$, $\hat{i}_t$) is equal to ($\hat{\Psi}_{sDFVC}$, $\hat{i}_{tDFVC}$). The $\hat{\Psi}_{sDFVC}$ and $\hat{i}_{tDFVC}$ are the observed flux amplitude and t-axis current by voltage model flux observer [26], [24]. The stator flux vector and t-axis current can be observed by voltage model flux observer with higher accuracy since the voltage amplitude is relatively large [26]. In this way, accurate DFVC can be achieved. Since the field weakening control can be directly achieved by limiting the reference flux amplitude through (15), the proposed control scheme inherits the advantages of the f-t frame based control schemes in field weakening region.

TABLE 1. IPMSM parameters.

Number of pole-pairs	3
Phase resistance	51.2 mΩ
Continuous/Maximum current	58.5/118 A
Peak power at base speed	10 kW
DC link voltage	120 V
Base/maximum speed	1350/4500 r/min
Continuous/peak torque	35.5/70 N·m
Peak power at maximum speed	7 kW

It worth to notice that there are two MTPA look-up tables in Fig. 2, which seems to increase the control scheme's complexity. However, the MTPA look-up table 1 and 2 can be obtained simultaneously in the same group of tests at a motor speed ω_t which is between ω_1 and the base speed ω_b by varying d-axis currents with same current amplitudes until the maximum torques are reached. In this way, the accurate optimal d-axis current for a given current amplitude can be measured and the accurate MTPA flux amplitude can be observed by the voltage model flux observer at the same time. By testing different current amplitudes or torque command, the MTPA d-axis currents and the MTPA flux amplitudes for look-up table 1 and 2 can be mapped, respectively. Moreover, due to the d- and q-axis currents for field weakening control depend on both torque and speed, the look-up tables for conventional FOC are usually 2 dimensional. However, since the proposed control scheme only adopts FOC for MTPA operation which is independent of speed, the look-up table 1 and 2 in Fig. 2 are 1 dimensional. Therefore, the generation of the look-up table 1 and 2 for the proposed control scheme is actually much easier than that of conventional FOC.

The error of the voltage model flux observer is related to motor speed [29]. When motor speed is low, especially close to zero, the stator voltage amplitude is small and the error of voltage model flux observer is relatively large because of the estimation errors of the voltage drop on the inverter or on the motor winding resistance, which is always inevitable. Due to the sensitivity of the f-t frame based MTPA control schemes to the errors of flux amplitude as mentioned in Section II part A, if the optimal flux amplitudes for MTPA operation are obtained by tests at a high speed through the voltage model flux observer, the MTPA control accuracy may be significantly deteriorated at low speed, and vice versa. However, the proposed integrated control scheme only adopts the f-t frame based control scheme for MTPA operation within a small speed range close to the based speed which is the maximum speed for MTPA operation. In this way, the error of the voltage model flux observer can be minimized. Moreover, due to the speed range in which the f-t frame based control scheme is adopted for MTPA operation is relatively narrow,

i.e., between ω_1 and the based speed, the influence of the flux observer accuracy variation due to the motor speed variation is also limited.

C. TRANSITION BETWEEN FOC AND DFVC

According to Fig. 2, for a given reference torque, two pairs of reference flux amplitudes, (Ψ^*_{sFOC}, Ψ^*_{sDFVC}), and reference t-axis currents, (i^*_{tFOC}, i^*_{tDFVC}), are generated for the FOC and the DFVC, respectively. In order to have a smooth transition between the two control schemes, a transition region, from ω_1 to ω_2, and vice versa, is defined as shown in Fig. 3.

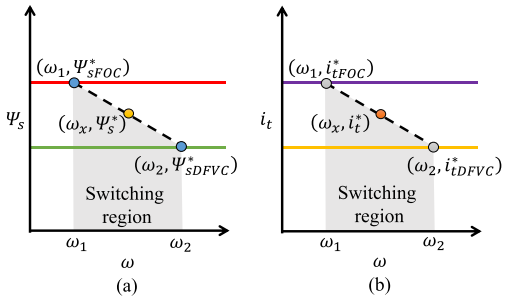

FIGURE 3. Linear interpolation in the transition region.

When the speed is below ω_1, Ψ^*_{sFOC} and i^*_{tFOC} generated for the FOC is adopted as the reference flux amplitude and t-axis current. When the speed is above ω_2, Ψ_{sDFVC} and i_{tDFVC} generated for the DFVC is adopted. When the speed ω_x is between the two, i.e., $\omega_1 < \omega_x < \omega_2$, the reference flux amplitude and t-axis current can be generated from the linear interpolation given in (29) and (30).

$$\Psi^*_s = \frac{\omega_2 - \omega_x}{\omega_2 - \omega_1}\Psi^*_{sFOC} + \frac{\omega_x - \omega_1}{\omega_2 - \omega_1}\Psi^*_{sDFVC} \tag{29}$$

$$i^*_t = \frac{\omega_2 - \omega_x}{\omega_2 - \omega_1} i^*_{tFOC} + \frac{\omega_x - \omega_1}{\omega_2 - \omega_1} i^*_{tDFVC} \tag{30}$$

Similarly, two pairs of observed flux amplitudes, ($\hat{\Psi}_{sFOC}$, $\hat{\Psi}_{sDFVC}$), and observed t-axis currents, ($\hat{i}_{tFOC}$, $\hat{i}_{tDFVC}$), shown in Fig. 2, are employed in the feedback loops of the proposed control scheme. When the speed is below ω_1, the observed $\hat{\Psi}_s$ and $\hat{i}_t$ are equal to $\hat{\Psi}_{sFOC}$ and $\hat{i}_{tFOC}$, respectively. When the speed is above ω_2, the $\hat{\Psi}_s$ and $\hat{i}_t$ are equal to $\hat{\Psi}_{sDFVC}$ and $\hat{i}_{tDFVC}$, respectively. If the speed is in between the two, $\hat{\Psi}_s$ and $\hat{i}_t$ are generated from the linear interpolation given in (31) and (32).

$$\hat{\Psi}_s = \frac{\omega_2 - \omega_x}{\omega_2 - \omega_1} \hat{\Psi}_{sFOC} + \frac{\omega_x - \omega_1}{\omega_2 - \omega_1}\hat{\Psi}_{sDFVC} \tag{31}$$

$$\hat{i}_t = \frac{\omega_2 - \omega_x}{\omega_2 - \omega_1} \hat{i}_{tFOC} + \frac{\omega_x - \omega_1}{\omega_2 - \omega_1}\hat{i}_{tDFVC} \tag{32}$$

Therefore, a smooth transition between the two control schemes can be achieved.

D. VOLTAGE MODEL FLUX OBSERVER

In this paper, a voltage model flux observer which is machine parameter independent is adopted, however, other kinds of observers are also possible for the proposed control scheme. The voltage model is given by (33) and (34).

$$\vec{\Psi}_s = \frac{1}{s}\left(\vec{v}_a - R\vec{I}_\alpha\right) \tag{33}$$

$$\Psi_s = \frac{E}{\omega_e} \tag{34}$$

where $\vec{\Psi}_s$ is the flux vector, $\vec{v}_a$ is the stator voltage vector, $\vec{I}_\alpha$ is the current vector. According to (33), the flux vector can be obtained by integration of the voltage vector. However, in practice, since the pure integration is always suffered from the integrator drift, a low-pass filters together with phase angle and magnitude compensations are always utilized instead of the integrator. The block diagram of the flux observer is shown in Fig. 4, $\vec{v}^*_a$ is the reference voltage vector, E is the EMF voltage amplitude, ω_e is the electrical speed, ω_c is the cut-off frequency of the low-pass filter, θ_e is the angular displacement of d-axis with respect to α-axis.

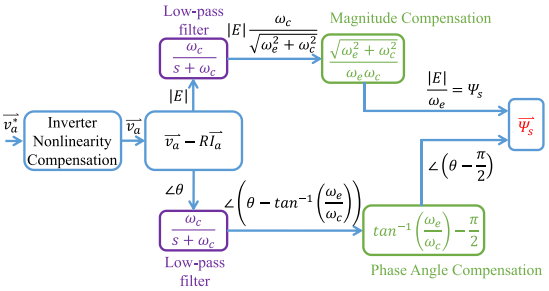

FIGURE 4. The flux observer.

IV. SIMULATION RESULTS

Simulations were performed based on a prototype IPMSM drive system. The motor specification is given in Table 1 and it is designed for distributed traction of a micro-size electric vehicle with peak power of 10 kW at the base speed of 1350 r/min. The d- and q-axis inductances and the permanent magnet flux linkage of the machine are highly non-linear and vary significantly with currents because of magnetic saturation. Given that the up limit of the transition speed should be below the based speed, the ω_1 and ω_2 in Fig. 3 are set to 800 r/min and 900 r/min, respectively. The L_d, L_q and Ψ_m in for FOC are set to their nominal values, i.e., 0.64 mH, 1.84 mH and 0.1132 Wb, respectively.

A. ACHIEVE FOC IN DFVC FRAME

In order to verify the FOC achieved in DFVC frame when speed is below ω_1, simulations were first performed by varying d- and q-axis reference currents from 0 A to the maximum current, i.e., 120 A, at 400 r/min, repetitively. The simulation results of the reference and resultant d- and q-axis currents of the proposed control scheme are shown in Fig. 5. It can be seen from Fig. 5, the resultant d- and q-axis currents always follow the reference d- and q-axis currents accurately even with nominal motor parameters, which demonstrates that the

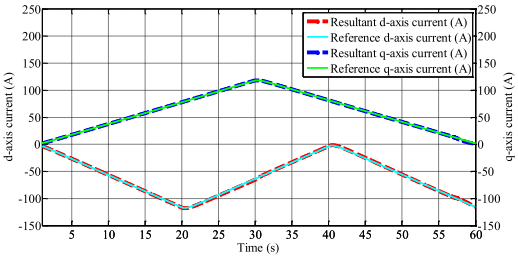

FIGURE 5. Reference and resultant d- and q-axis currents of the proposed control scheme at 400 r/min.

reference d- and q-axis current can be controlled through Ψ_s^* and i_t^*.

Since the $(\hat{\Psi}_{sFOC}, \hat{\hat{i}}_{tFOC})$ and $(\Psi^*_{sFOC}, i^*_{tFOC})$ in Fig. 2 were calculated based on machine parameters through (3) and (17), in order to study the influence of machine parameter errors on the FOC control performance in the DFVC frame, an error varied from -10% to 10% of the Ψ_m amplitude was injected into the Ψ_m which is the dominant component of $\hat{\Psi}_{sFOC}$ and Ψ^*_{sFOC}. The simulation results of the reference torque, resultant torque and the percentages of error injected into Ψ_m are illustrated in Fig. 6.

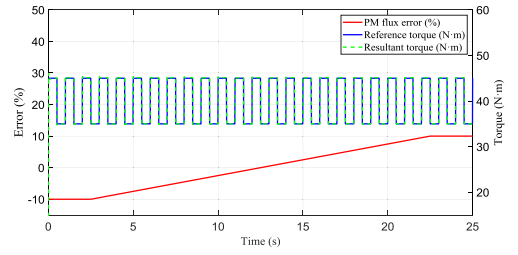

FIGURE 6. Reference and resultant torque of the proposed control scheme when errors were injected into Ψ_m at 400 r/min.

As can be seen from Fig. 6, although the error injected into the Ψ_m varied from -10% to 10%, the resultant torque followed the reference torque accurately. This was due to the fact that the error in $(\Psi^*_{sFOC}, i^*_{tFOC})$ caused by the inaccurate Ψ_m was compensated by the current model based flux observer in which $\hat{\Psi}_{sFOC}$ and $\hat{\hat{i}}_{tFOC}$ were generated based on the same Ψ_m. As a result, the resultant (i_d, i_q) essentially followed (i_d^*, i_q^*), which make the resultant torque followed the reference torque accurately.

B. PERFORMANCE OF THE PROPOSED CONTROL SCHEME DURING SPEED AND TORQUE CHANGING

In order to verify the performance of the proposed integrated control scheme during speed and torque changing, simulations were performed with the rotor speed stepped from 100 r/min ($< \omega_1$) to 1000 r/min ($> \omega_2$) in every 5 seconds before t = 30 s. After t = 30 s, the rotor speed stepped between 810 r/min and 890 r/min, i.e., varied between ω_1 and ω_2, in every 5 seconds. In this way, the proposed control scheme switched between FOC mode and DFVC mode continuously before t = 30 s and the rotor speed stepped continuously in the transition region after t = 30 s. Moreover, the reference torque stepped from 10 N·m to 50 N·m in every 10 s. The resultant torque, reference torque and rotor speed are shown in Fig. 7. As shown in Fig. 7, the resultant torque always follows the reference torque no matter if the control mode switched or rotor speed varies in the transition region.

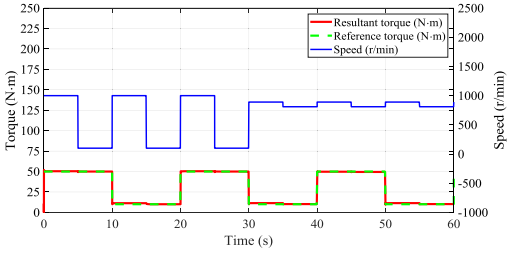

FIGURE 7. The resultant torque, reference torque and rotor speed when rotor speed and torque varies.

The three-phase current waveforms around t = 20 s corresponding to the operating condition illustrated in Fig. 7, i.e., when torque stepped from 10 N·m to 50 N·m and rotor speed stepped from 100 r/min to 1000 r/min, are shown in Fig. 8.

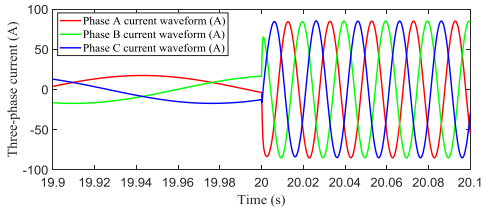

FIGURE 8. The three-phase current waveforms around t = 20 s corresponding to the operating condition illustrated in Fig. 7.

As can be seen from Fig. 8, the three-phase current waveforms are sinusoidal before and after the step change of the speed and torque. During the speed and torque step, the three-phase current waveforms changed promptly. This is due to the proposed control scheme is actually implemented in the f-t reference frame, which directly regulates the flux linkage through voltage vector instead of regulating the currents. It worth to notice that for most applications, electric vehicle traction, in particular, a step-change in speed will not occur due to drive system inertia or large mass. Therefore, conditions which are worse than that illustrated in Fig. 7 will not happen practically.

C. CONTROL PERFORMANCE IN TRANSITION REGION

The control performance of the proposed integrated control scheme in the transition region is also studied. The reference torque was set to 45 N·m and rotor speed varied from 700 r/min ($< \omega_1$) to 1000 r/min ($> \omega_2$) gradually. Moreover, errors were deliberately injected in i_q^* and i^*_{tDFVC} of Fig. 2 so that when the motor was controlled in FOC mode, the resultant torque was 48 N·m. Whereas when the motor was controlled in DFVC mode, the resultant torque

was 42 N·m. The simulation result of the proposed control scheme is shown in Fig. 9. As shown in Fig. 9, when the rotor speed is below ω_1, the motor was controlled in FOC mode, the resultant torque was 48 N·m. When the rotor speed is above ω_2, the motor was controlled in DFVC mode and the resultant torque was 42 N·m. When the rotor speed was between ω_1 and ω_2, i.e., in transition region, the resultant torque was between 48 N·m and 42 N·m. This simulation results illustrate that the torque control accuracy of the proposed control scheme in transition region is between the accuracy of FOC and DFVC.

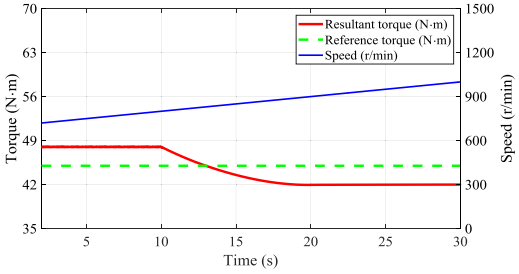

FIGURE 9. Control performance of the proposed integrated control scheme in the transition region when the speed varies from 700 r/min to 1000 r/min.

V. EXPERIMENT RESULTS

The proposed integrated control scheme has been implemented and tested on a prototype IPMSM drive whose specifications are given in Table 1. The prototype machine was mounted via a high precision inline torque transducer on the test-rig and loaded by the dynamometer as shown in Fig. 10. During the tests, the IPMSM operated in torque control mode with its speed controlled by the dynamometer. The inverter switching frequency was 8 kHz. The L_d, L_q and Ψ_m in (3) and (34) were set to their nominal values, i.e., 0.64 mH, 1.84 mH and 0.1132 Wb, respectively. The MTPA look-up table 1 and 2 in Fig. 2 were the same as the ones in the simulation part. The ω_1 and ω_2 in Fig. 3 were set to 800 r/min and 900 r/min, respectively.

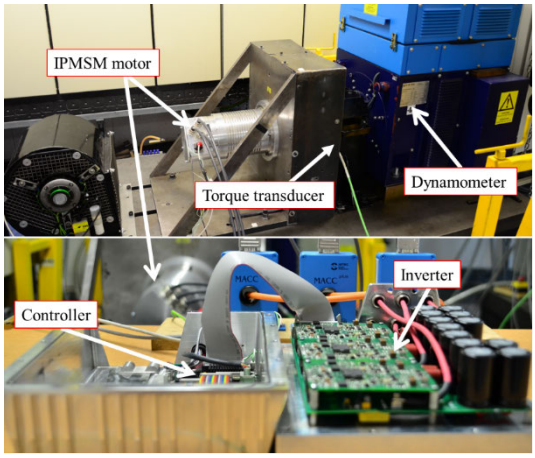

FIGURE 10. IPMSM test rig and the motor controller.

A. FOC AT LOW SPEED

The test was first carried out when the speed was below 800 r/min, and the motor was effectively controlled by the FOC scheme through the f-t frame. To illustrate the performance of the proposed control scheme, the motor drive was tested at 400 r/min with step changes in reference torque. Fig. 11 shows the reference d-axis current and measured d-axis current when the reference torque was stepped from 30 N·m to 35 N·m. As can be seen, the measured d-axis current follows the reference d-axis current generated by the look-up table 1 for FOC accurately.

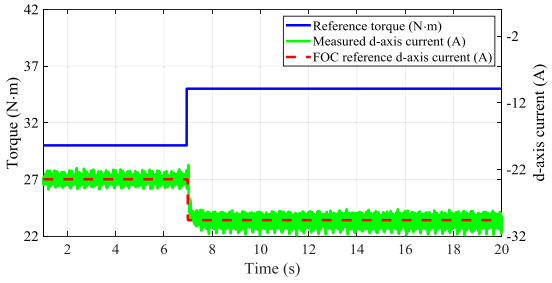

FIGURE 11. Reference torque, FOC reference d-axis current and measured d-axis current when the reference torque stepped from 30 N·m to 35 N·m at 400 r/min.

The reference and measured q-axis currents under the same operating conditions as Fig. 11 are compared in Fig. 12. The accurate q-axis current control can also be observed. The measured torque is shown in Fig. 18.

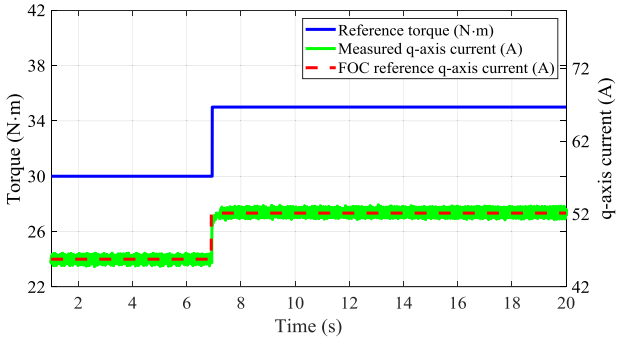

FIGURE 12. FOC reference q-axis current, measured q-axis current and reference torque at 400r/min with the reference torque stepped from 30 N·m to 35 N·m.

B. TRANSITION BETWEEN FOC AND DFVC

When the motor is operating in the transition region, i.e., from 800 r/min to 900 r/min, the proposed control scheme is a linear combination of the FOC scheme and the DFVC scheme through (29)–(32).

To verify the performance of the proposed control scheme in the transition region, the motor drive was tested at 850 r/min. Fig. 13 shows the reference d-axis current, i_d^*, generated by the look-up table 1 in Fig. 2 and the measured d-axis current when the reference torque changes in step

from 30 N·m to 35 N·m. Due to the errors of the nominal machine parameters, (Ψ^*_{sFOC}, i^*_{tFOC}) calculated by (3) and (17) is not equal to (Ψ^*_{sDFVC}, i^*_{tDFVC}). According to (29), (30) and (3), (17), the reference d-axis current for (Ψ^*_{sFOC}, i^*_{tFOC}) is different from that corresponding to the (Ψ^*_s, i^*_t). Hence, the resultant d-axis current of the proposed control scheme is not equal to the i^*_d generated by the look-up table 1, i.e., the MTPA d-axis current, in the transition region as shown in Fig. 13. However, due to the proposed integrated control scheme directly controls (Ψ^*_s, i^*_t) in Fig. 2, therefore, even the (Ψ^*_s, i^*_t) is different from (Ψ^*_{sFOC}, i^*_{tFOC}) or (Ψ^*_{sDFVC}, i^*_{tDFVC}), the ($\hat{\Psi}_s$, $\hat{i}_t$) can be still controlled to follow (Ψ^*_s, i^*_t). The measured torque is shown in Fig. 18. The error between the reference d-axis current and the measured d-axis current shown in Fig. 13 can be minimized if accurate machine parameters are adopted in (3) and (17) instead of the nominal values.

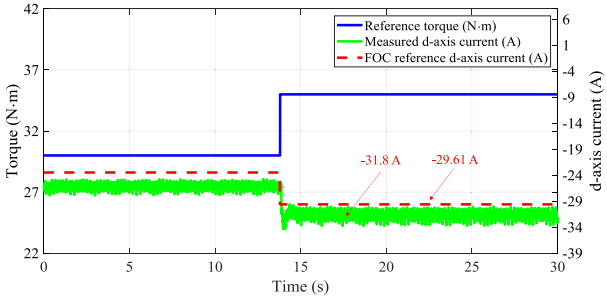

FIGURE 13. Reference torque, measured d-axis current and FOC reference d-axis current when the reference torque stepped from 30 N·m to 35 N·m at 850 r/min.

Fig. 14 shows the observed flux amplitude, $\hat{\Psi}_s$, and the Ψ^*_{sDFVC} (from look-up table 2) under the same operating condition as in Fig. 13, Similarly, the observed flux amplitude of the proposed control scheme is not equal to the Ψ^*_{sDFVC}, i.e., the MTPA stator flux amplitude, in the transition region. From Fig. 13 and Fig. 14, it can be seen that a 2.7% error in flux amplitude causes a 7.3% error in the d-axis current, this experimentally proves the derivations in Section II part A.

Tests were also performed by varying speed from 1100 r/min to 400 r/min and back to 1100 r/min with 20 N·m

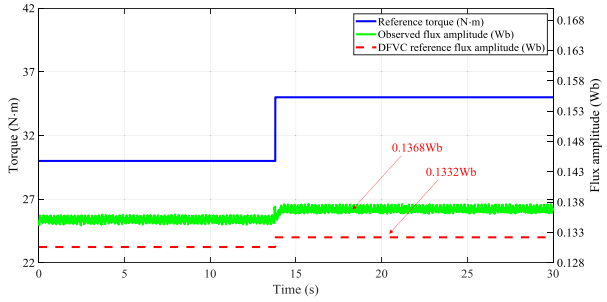

FIGURE 14. Reference torque, observed flux amplitude and DFVC reference flux amplitude when the reference torque stepped from 30 N·m to 35 N·m at 850 r/min.

reference torque. As shown in Fig. 15, smooth transitions from the DFVC to the FOC and vice versa can be observed.

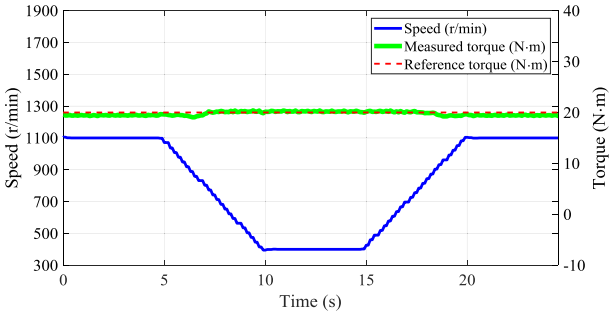

FIGURE 15. Transitions between DFVC and FOC with 20 N·m reference torque.

The three-phase current waveforms measured by oscilloscope at 20 N·m torque and speed around 850 r/min when the motor speed was varying from 400 r/min to 1100 r/min are shown in Fig. 16.

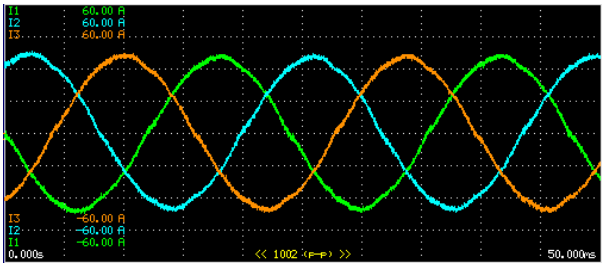

FIGURE 16. Measured three-phase current waveforms at 20 N·m torque around speed of 850 r/min.

As can be seen from Fig. 16, although the motor is operating around the speed of 850 r/min, i.e., within the transition region shown in Fig. 16, the resultant current waveforms are still sinusoidal, which indicates that the proposed control scheme integrates the FOC and DFVC successfully.

C. DFVC AT HIGH SPEED

When speed is above 900 r/min, the proposed control scheme becomes a conventional DFVC as proposed in [13], [22], [23]. To illustrate the performance of the proposed control scheme, the motor drive was tested at 1000 r/min. Fig. 17 shows the observed flux amplitude and

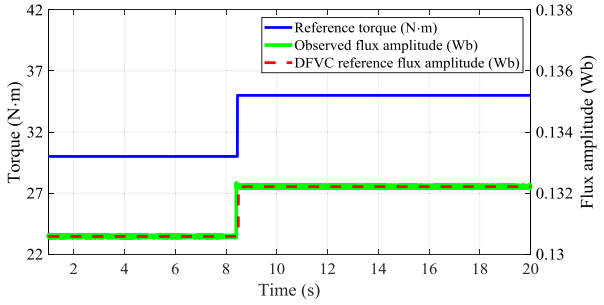

FIGURE 17. Reference torque, observed flux amplitude and DFVC reference flux amplitude when the reference torque stepped from 30 N·m to 35 N·m at 1000 r/min.

reference flux amplitude of the proposed control scheme when reference torque steps from 30 N·m to 35 N·m. As shown in Fig. 17, due to the motor drive is only controlled by DFVC, the observed flux amplitude follows the reference torque accurately. The measured torque is shown in Fig. 18.

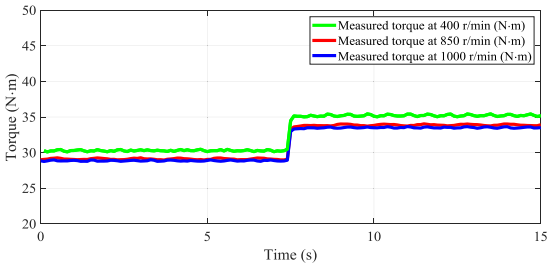

FIGURE 18. Measured torque at 400 r/min, measured torque at 850 r/min and measured torque at 1000 r/min when torque reference steps from 30 N·m to 35 N·m.

Fig. 18 shows the measured torque when reference torque steps from 30 N·m to 35 N·m at 400 r/min, 850 r/min and 1000 r/min, respectively. As shown in Fig. 18 the resultant torques in transition region ($\omega_m = 850$ r/min) are always around the torques generated by FOC and DFVC due to the (Ψ_s^*, i_t^*) and $(\hat{\Psi}_s, \hat{i}_t)$ are calculated from (29)-(32). The slight errors in the measured torque when the motor is operating at high speeds are due to the mechanical friction and the errors of flux observer.

D. FIELD WEAKENING CONTROL

In the field weakening region, the rotor speed is above ω_2, conventional DFVC is adopted by the proposed control scheme and the stator flux amplitude is directly limited by (15). The performance of the proposed control scheme in field weakening region was tested by experiments. Fig. 19 shows the measured torque, reference torque, reference flux amplitude and observed flux amplitude when the reference torque stepped from 15 N·m to 20 N·m at 2700 r/min (two times base speed). As shown in Fig. 19, due to the motor being controlled by DFVC, the reference flux amplitude is equal to the observed flux amplitude. The small error between the reference and measured torques is due to the frictional torque of the motor and flux observer error.

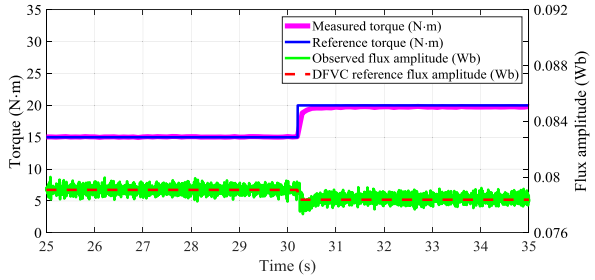

FIGURE 19. Reference torque, measured torque, reference flux amplitude and observed flux amplitude with torque stepped from 15 N·m to 20 N·m at 2700 r/min.

Fig. 20 shows the resultant voltage amplitude, maximum voltage amplitude and resultant d-axis current under the same operating condition as in Fig. 19. As shown in Fig. 19 and Fig. 20, although errors can be observed in resultant torque, the resultant voltage amplitude is always kept at the maximum voltage amplitude and the proposed control scheme inherits the advantages of DFVC in field weakening region.

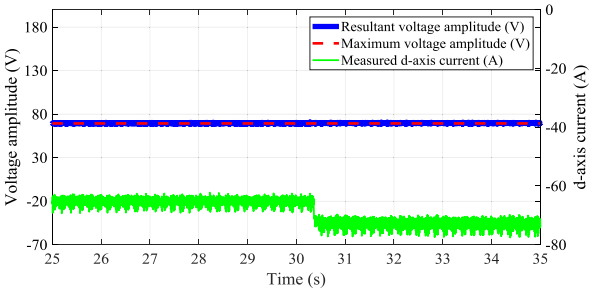

FIGURE 20. Resultant voltage amplitude, maximum voltage amplitude and resultant d-axis current when reference torque steps from 15 N·m to 20 N·m at 2700 r/min.

VI. CONCLUSION

This paper proposed a novel integrated control scheme which combines FOC scheme with DFVC. The proposed control scheme inherits the advantages of both FOC and DFVC but avoids the disadvantages of the two conventional control schemes. The proposed control scheme is verified by simulations and experiments. Simulation and experiment results show that the proposed control scheme not only control IPMSM drive follows reference d- and q-axis currents accurately at low speed, but also manipulate and limit flux amplitude directly at high speed. The smooth transition between FOC and DFVC also verified by experiments. Therefore, the proposed control scheme could achieve an accurate MTPA control in constant torque region and a better field weakening performance in constant power region. Meanwhile the complex look-up tables for FOC in field weakening region and the difficulties in observing flux vector at low speed are also avoided.

REFERENCES

[1] T. Miyajima, H. Fujimoto, and M. Fujitsuna, "A precise model-based design of voltage phase controller for IPMSM," *IEEE Trans. Power Electron.*, vol. 28, no. 12, pp. 5655–5664, Dec. 2013.

[2] T. Sun, J. Wang, and X. Chen, "Maximum torque per ampere (MTPA) control for interior permanent magnet synchronous machine drives based on virtual signal injection," *IEEE Trans. Power Electron.*, vol. 30, no. 9, pp. 5036–5045, Sep. 2015.

[3] T. Sun and J. Wang, "Extension of virtual-signal-injection-based MTPA control for interior permanent-magnet synchronous machine drives into the field-weakening region," *IEEE Trans. Ind. Electron.*, vol. 62, no. 11, pp. 6809–6817, Nov. 2015.

[4] S. Bolognani, S. Calligaro, and R. Petrella, "Adaptive flux-weakening controller for interior permanent magnet synchronous motor drives," *IEEE J. Emerg. Sel. Topics Power Electron.*, vol. 2, no. 2, pp. 236–248, Jun. 2014.

[5] C. Xia, S. Li, Y. Shi, X. Zhang, Z. Sun, and W. Yin, "A non-smooth composite control approach for direct torque control of permanent magnet synchronous machines," *IEEE Access*, vol. 7, pp. 45313–45321, 2019.

[6] T. Yuan, D. Wang, X. Wang, X. Wang, and Z. Sun, "High-precision servo control of industrial robot driven by PMSM-DTC utilizing composite active vectors," *IEEE Access*, vol. 7, pp. 7577–7587, 2019.
[7] B. Cheng and T. R. Tesch, "Torque feedforward control technique for permanent-magnet synchronous motors," *IEEE Trans. Ind. Electron.*, vol. 57, no. 3, pp. 969–974, Mar. 2010.
[8] C. Cavallaro, A. O. DiTommaso, R. Miceli, A. Raciti, G. R. Galluzzo, and M. Trapanese, "Efficiency enhancement of permanent-magnet synchronous motor drives by online loss minimization approaches," *IEEE Trans. Ind. Electron.*, vol. 52, no. 4, pp. 1153–1160, Aug. 2005.
[9] R. Nalepa and T. Orlowska-Kowalska, "Optimum trajectory control of the current vector of a nonsalient-pole PMSM in the field-weakening region," *IEEE Trans. Ind. Electron.*, vol. 59, no. 7, pp. 2867–2876, Jul. 2012.
[10] Y. Ren, Z. Q. Zhu, and J. Liu, "Direct torque control of permanent-magnet synchronous machine drives with a simple duty ratio regulator," *IEEE Trans. Ind. Electron.*, vol. 61, no. 10, pp. 5249–5258, Oct. 2014.
[11] Y. Ren and Z. Q. Zhu, "Enhancement of steady-state performance in direct-torque-controlled dual three-phase permanent-magnet synchronous machine drives with modified switching table," *IEEE Trans. Ind. Electron.*, vol. 62, no. 6, pp. 3338–3350, Jun. 2015.
[12] C. Xia, J. Zhao, Y. Yan, and T. Shi, "A novel direct torque control of matrix converter-fed PMSM drives using duty cycle control for torque ripple reduction," *IEEE Trans. Ind. Electron.*, vol. 61, no. 6, pp. 2700–2713, Jun. 2014.
[13] G. Pellegrino, E. Armando, and P. Guglielmi, "Direct-flux vector control of IPM motor drives in the maximum torque per voltage speed range," *IEEE Trans. Ind. Electron.*, vol. 59, no. 10, pp. 3780–3788, Oct. 2012.
[14] M. N. Uddin, T. S. Radwan, and M. A. Rahman, "Performance of interior permanent magnet motor drive over wide speed range," *IEEE Trans. Energy Convers.*, vol. 17, no. 1, pp. 79–84, Mar. 2002.
[15] C.-T. Pan and S.-M. Sue, "A linear maximum torque per ampere control for IPMSM drives over full-speed range," *IEEE Trans. Energy Convers.*, vol. 20, no. 2, pp. 359–366, Jun. 2005.
[16] Y. Inoue, S. Morimoto, and M. Sanada, "Comparative study of PMSM drive systems based on current control and direct torque control in flux-weakening control region," *IEEE Trans. Ind. Appl.*, vol. 48, no. 6, pp. 2382–2389, Nov. 2012.
[17] M. Tursini, E. Chiricozzi, and R. Petrella, "Feedforward flux-weakening control of surface-mounted permanent-magnet synchronous motors accounting for resistive voltage drop," *IEEE Trans. Ind. Electron.*, vol. 57, no. 1, pp. 440–448, Jan. 2010.
[18] S.-Y. Jung, J. Hong, and K. Nam, "Current minimizing torque control of the IPMSM using Ferrari's method," *IEEE Trans. Power Electron.*, vol. 28, no. 12, pp. 5603–5617, Dec. 2013.
[19] A. Consoli, G. Scarcella, G. Scelba, and A. Testa, "Steady-state and transient operation of IPMSMs under Maximum-Torque-per-Ampere control," *IEEE Trans. Ind. Appl.*, vol. 46, no. 1, pp. 121–129, Nov. 2010.
[20] K. D. Hoang, J. Wang, M. Cyriacks, A. Melkonyan, and K. Kriegle, "Feedforward torque control of interior permanent magnet brushless AC drive for traction applications," in *Proc. IEEE IEMDC.*, May 2013, pp. 152–159.
[21] B. Stumberger, G. Stumberger, D. Dolinar, A. Hamler, and M. Trlep, "Evaluation of saturation and cross-magnetization effects in interior permanent-magnet synchronous motor," *IEEE Trans. Ind. Appl.*, vol. 39, no. 5, pp. 1264–1271, Sep. 2003.
[22] G. Pellegrino, E. Armando, and P. Guglielmi, "Direct flux field-oriented control of IPM drives with variable DC link in the field-weakening region," *IEEE Trans. Ind. Appl.*, vol. 45, no. 5, pp. 1619–1627, 2009.
[23] G. Pellegrino, R. I. Bojoi, and P. Guglielmi, "Unified direct-flux vector control for AC motor drives," *IEEE Trans. Ind. Appl.*, vol. 47, no. 5, pp. 2093–2102, Sep. 2011.
[24] T. Sun, J. Wang, and M. Koc, "Virtual signal injection-based direct flux vector control of IPMSM drives," *IEEE Trans. Ind. Electron.*, vol. 63, no. 8, pp. 4773–4782, Aug. 2016.
[25] G. Pellegrino, E. Armando, and P. Guglielmi, "Direct-flux field-oriented control of IPM motor drives with robust exploitation of the maximum torque per voltage speed range," in *Proc. IEEE Int. Symp. Ind. Electron.*, Jul. 2010, pp. 1271–1277.
[26] A. Yoo and S.-K. Sul, "Design of flux observer robust to interior permanent-magnet synchronous motor flux variation," *IEEE Trans. Ind. Appl.*, vol. 45, no. 5, pp. 1670–1677, Sep./Oct. 2009.
[27] T. Sun, "Efficiency optimised control of interior permanent magnet synchronous machine (IPMSM) drives for electric vehicle tractions," Ph.D. dissertation, Dept. Electron. Elect. Eng., The Univ. Sheffield, Sheffield, U.K., 2016.
[28] T. Sun, M. Koc, and J. Wang, "MTPA control of IPMSM drives based on virtual signal injection considering machine parameter variations," *IEEE Trans. Ind. Electron.*, vol. 65, no. 8, pp. 6089–6098, Aug. 2018.
[29] M. Koc, J. Wang, and T. Sun, "Performance improvement of direct torque controlled interior mounted permanent magnet drives by employing a linear combination of current and voltage based flux observers," *IET Power Electron.*, vol. 9, no. 10, pp. 2052–2059, Aug. 2016.

TIANFU SUN (Member, IEEE) was born in China. He received the B.Eng. degree in mechanical engineering and the M.Sc. degree in civil engineering from the Dalian University of Technology, Dalian, China, in 2009 and 2012, respectively, and the Ph.D. degree in electrical and electronics engineering from The University of Sheffield, Sheffield, U.K., in 2016.

From 2016 to 2017, he was with the Department of Electronics and Electrical Engineering, The University of Sheffield, where he was a Postdoctoral Research Fellow. He is currently working as an Associate Professor and a Senior Engineer in electric drives with the Shenzhen Institutes of Advanced Technology, Chinese Academy of Sciences, Shenzhen, China. He is the Director of the Shenzhen Key Laboratory of Electric Vehicle Powertrain Platform and Safety Technology. His current research interests include power electronics and motor drives.

JIABIN WANG (Senior Member, IEEE) received the B.Eng. and M.Eng. degrees from the Jiangsu University of Science and Technology, Zhenjiang, China, in 1982 and 1986, respectively, and the Ph.D. degree from the University of East London, London, U.K., in 1996, all in electrical and electronics engineering.

From 1986 to 1991, he was with the Department of Electrical Engineering, Jiangsu University of Science and Technology, where he was appointed as a Lecturer, in 1987, and an Associate Professor, in 1990. He was a Postdoctoral Research Associate at The University of Sheffield, Sheffield, U.K., from 1996 to 1997, and a Senior Lecturer at the University of East London, from 1998 to 2001. He is currently a Professor of electrical engineering with The University of Sheffield. His research interests range from motion control and electromechanical energy conversion to electric drives for applications in automotive and renewable energy. He is a Fellow of the IET.

CHENGLI JIA was born in China. He received the B.Eng. degree in mechanical design, manufacturing, and automation from Yanshan University, Hebei, China, in 2018. He is currently working as an Intern with the Shenzhen Institutes of Advanced Technology, Chinese Academy of Sciences. His current research interests are motor drives.

LEI PENG (Member, IEEE) received the M.S. and Ph.D. degrees in computer science from the University of Electronic Science and Technology of China, in 2003 and 2009, respectively. He is currently an Associate Research Fellow of the Shenzhen Institutes of Advanced Technology, Chinese Academy of Sciences. His research interests include electric vehicles and their related applications.